Reflectivity computation from separated wavefields: application on the Sigsbee2B example

Alba Ordoñez, PGS Geophysical AS/UiO, Walter Söllner, PGS Geophysical AS, Tilman Klüver, PGS Geophysical AS and Leiv J. Gelius, UiO*

Summary

This paper discusses imaging using the wavefield separated into upgoing and downgoing components and including primaries and multiples. We image the reflectivity by solving Fredholm integral equations at every depth level of the image, after extrapolating the wavefields with a one-way wave equation propagator. The reflectivity, or reflected wavefield in the hypothetical experiment with point sources and receivers at the image level, is determined free of multiple scattering from the overburden. We also show how the reflectivity, obtained by inverting the matrix form of the Fredholm integral equations, can be extended to angle-dependent reflectivity at the image point.

Introduction

It has long been recognized that multiples provide valuable structural information when they are handled in a correct way in imaging (e.g., Berkhout, 1985; Mujis et al., 2007). In this paper, we consider the complete wavefield in imaging, including primaries and multiples.

To properly account for multiple scattering in imaging, the computation of the reflectivity at every image level appears as an option. The reflectivity can be recovered from a Fredholm integral equation of the first kind defined in the frequency-space domain, in terms of upgoing and downgoing separated wavefields (see e.g. Amundsen, 2001; Ordoñez et al., 2014a and 2014b). An inversion of the matrix form of this integral problem at every image level gives the reflectivity, where cross-talk caused by the physical overburden should be eliminated.

Here, we first review previous related work using upgoing and downgoing separated wavefields (Claerbout, 1971; Whitmore et al., 2010; Lu et al., 2011; Ordoñez et al., 2014a and 2014b). Then, we compute the reflectivity matrix by integral inversion for a sediment section of the Sigsbee2B model (Paffenholz et al., 2002). By choosing a convenient subset of the reflectvity matrix, we build a structural subsurface image, that we compare with the result from the migration scheme based on application of a cross-correlation imaging condition. Moreover, we analyse the angle-dependency of the reflectivity and we retrieve the data at virtual sources and receivers located in the subsurface, above arbitrary image levels.

Imaging using up and downgoing wavefields

One popular approach to imaging consists of downward extrapolating the receiver and source wavefields before applying an imaging condition (Claerbout, 1971). In wave-equation migration, one of the imaging conditions most commonly used in practice is defined in terms of a cross-correlation of the receiver and source pressure wavefields, according to (Claerbout, 1971):

$$I_c(\mathbf{x})=\sum_{\mathbf{x_s}} \sum_{\omega} U^P(\omega,\mathbf{x},\mathbf{x_s})D^{P^*}(\omega,\mathbf{x},\mathbf{x_s}), \quad (1)$$

where the transcript * denotes complex conjugation, $\mathbf{x}$ is the image position and $\mathbf{x_s}$ is the source position. The upgoing and downgoing pressure wavefields U^P and D^P are respectively used as receiver and source wavefields. Note that the summation over angular frequencies (ω) represents the extraction of the zero-time lag.

For migration considering primaries and multiples, ray path interactions caused by the physical overburden (i.e. cross-talk) should be suppressed as much as possible. Deconvolution has the potential to reduce the cross-talk over cross-correlation (e.g. Poole et al., 2010; Whitmore et al., 2010). Standard deconvolution imaging conditions are also defined in terms of pressure wavefields only. Guitton et al. (2007) and Lu et al. (2011), define a deconvolution imaging condition containing a smoothing operator $\langle\ \rangle$ and a constant ε to avoid division by small numbers:

$$I_d(\mathbf{x})=\sum_{\mathbf{x_s}} \sum_{\omega} \frac{U^P(\omega,\mathbf{x},\mathbf{x_s})D^{P^*}(\omega,\mathbf{x},\mathbf{x_s})}{\langle D^P(\omega,\mathbf{x},\mathbf{x_s})D^{P^*}(\omega,\mathbf{x},\mathbf{x_s})\rangle+\varepsilon}. \quad (2)$$

To further reduce the response of the physical overburden and properly collapse primaries and multiples in the same image, inverting for the reflected component of the impulse response (i.e. reflectivity) at every image level may appear as an option.

It is well known from the literature that the reflectivity can be recovered from a Fredholm integral equation of the first kind defined in the frequency-space domain (see e.g. Amundsen, 2001; Ordoñez et al., 2014a). Assuming that sufficient data are available, an inversion of the matrix form of the integral gives an estimate of the reflectivity matrix $\mathbf{R}$. For a single frequency and a single depth level, this equation is defined as follows (for details, refer to Ordoñez et al., 2014a and 2014b):

$$\mathbf{U^P} = \mathbf{R}\,\mathbf{D_f^{V_z}}. \quad (3)$$

We have introduced the filtered downgoing vertical velocity wavefield $D_f^{V_z}=-2i\omega\rho D^{V_z}$ (i being the imaginary unit and ρ the mass density) and defined the matrices $\mathbf{U^P}$, $\mathbf{R}$ and $\mathbf{D_f^{V_z}}$. Their rows correspond respectively to $U^P(\mathbf{x_r},\mathbf{x_s})$, $R(\mathbf{x_r},\mathbf{x})$ and $D_f^{V_z}(\mathbf{x},\mathbf{x_s})$ for a fixed receiver and variable source location and their columns represent the reciprocal case. Note that $\mathbf{x_r}$ is the receiver position. The matrix

DOI http://dx.doi.org/10.1190/segam2015-5828037.1

inversion to compute **R** corresponds to temporal and spatial deconvolution. In the following, we compute the reflectivity by solving a damped least-squares problem using Tikhonov regularization (Tikhonov et al., 1995; Berkhout and Verschuur, 2003; Wapenaar et al., 2008 and 2012). The reflectivity has a band-matrix structure (Verschuur and Berkhout, 2009) and the spatial structural information is essentially contained within a narrow band around the main diagonal. Note that this subset corresponds to coincident virtual sources and receivers in space (virtual zero-offset).

In the next numerical example, we use complete wavefields for imaging, i.e. the downgoing wavefield contains the direct downgoing wavefield from the source.

Sigsbee2B example

We have chosen a subset of the Sigsbee2B model (Figure 1a) for illustrative purpose. We focus particularly on the sediment section shown in the background velocity model

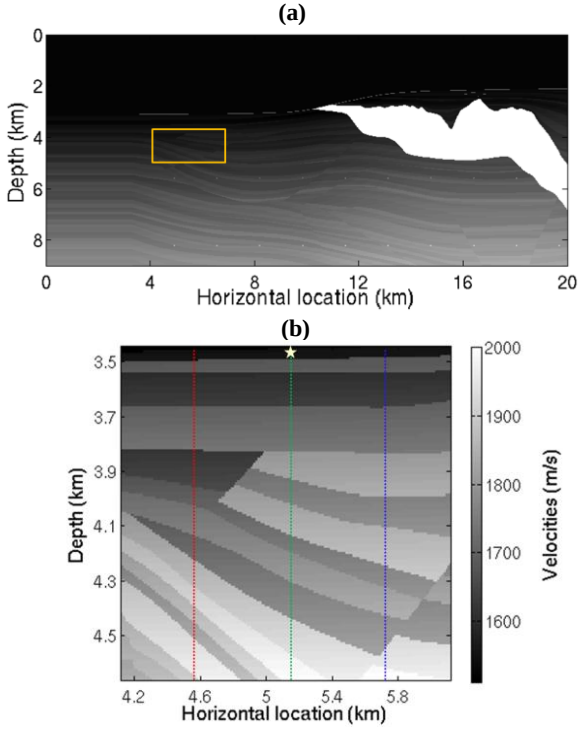

Figure 1: (a) Sigsbee2B model; the yellow rectangle indicates the target imaging area. (b) Backgound velocity model of the target imaging area. The colored dashed lines indicate the lateral positions along which we determine the common-midpoint migrated sections and angle gathers of Figure 4. The star corresponds to the depth level and lateral position where we generate the reflectivity wavefield of Figure 5a.

of Figure 1b. The target area is 1.1 km deep and 2.7 km wide. Split-spread data has been generated for 160 shots with 697 receivers each. Shot and receiver spacing were respectively 49.2 m and 24.6 m. Source and receiver depth was 24.6 m. By using modeled pressure measurements at two different depth levels, we computed the complete upgoing and downgoing wavefields (Posthumus, 1993). Figure 2 shows one shot record of the up (Figure 2a) and downgoing (Figure 2b) pressure data. Note that primary and multiple reflections are present in the data and the downgoing field contains the direct wavefield from the source (Figure 2b).

We compare the structural migrated section computed from the cross-correlation imaging condition of equation 1 to the one derived from our reflectivity method, where we have extracted the zero-time lag and the zero-offset response of the reflectivity (computed from equation 3). The different structural images of separated wavefields as well as the reflectivity matrix at a given depth level are displayed in Figure 3. Figure 3a shows the image obtained using migration with the cross-correlation imaging condition, and clearly shows the image of a multiple that is not properly accounted for in this imaging scheme. In Figure 3b, we build the image by integral inversion and present the section obtained after extracting for each depth level, the zero-time lag and selecting the main diagonal of the reflectivity matrix (Figure 3c). Note that we have eliminated the cross-talk previously observed.

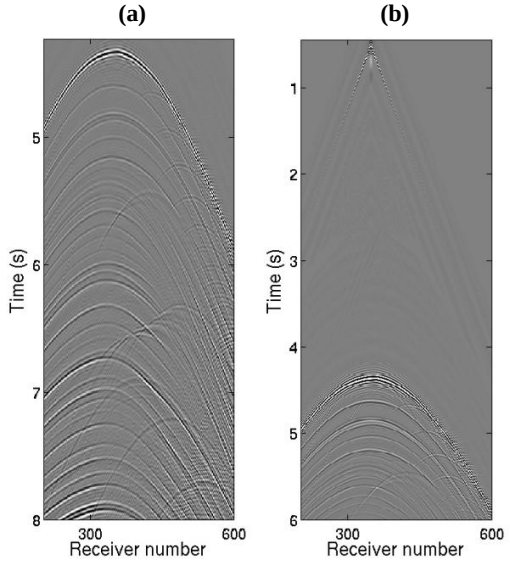

Figure 2: Deghosted upgoing (a) and downgoing (b) pressure wavefields at source 1. A scaling was applied to enhance the later events.

Beyond computing the structural migrated sections in depth-space from the reflectivity matrix, it is also possible

DOI http://dx.doi.org/10.1190/segam2015-5828037.1

to create angle-gathers. For each frequency and in the space domain, we selected three subsets of the reflectivity matrix perpendicular to the main diagonal (Figure 3c). Each of these subsets is associated with a virtual common-midpoint. It illuminates a narrow part of the model in space, but this information can be stretched to the angle domain. Following de Bruin et al. (1990) and Ordoñez et al. (2014b), (i) we transformed the selected subsets from the frequency-space to the frequency-wavenumber domain, (ii) then we stretched the obtained plane-wave reflection coefficients from the wavenumber-domain to the angle domain, and (iii) finally we performed a summation over frequencies (i.e. extraction of the zero time-lag). In Figure 1b, we indicate the lateral positions of the model along which we compute the common-midpoint migrated sections and the angle gathers. Note that in the migrated sections (Figure 4a, Figure 4c and Figure 4e), the energy of the different reflections is mainly focused in one point. This information is stretched to the angle domain and the true reflectors are horizontally aligned in the angle gather (Figure 4b, Figure 4d and Figure 4f).

Now, for a given lateral position, we construct a common shot gather of the reflectivity, which represents the wavefield at virtual sources and receivers located in the subsurface, above an imaging level. This is achieved in two steps: (i) for each frequency and for a given imaging level, we select a column of the reflectivity matrix computed using equation 3 and (ii) we perform an inverse Fourier transformation over the frequencies to obtain the sought after shot record of the reflectivity wavefield (in time). In Figure 5a, we display such a record obtained as if the source was at the position indicated by a star in Figure 1b (with a split-spread of receivers surrounding it). The events of the computed wavefield can directly be related to the migrated layers of the zero-offset section. Note that the four first reflections have their apex in the middle of the display (Figure 5a). This corresponds to the first four horizontal layers (Figure 5b). The other reflections have their apex

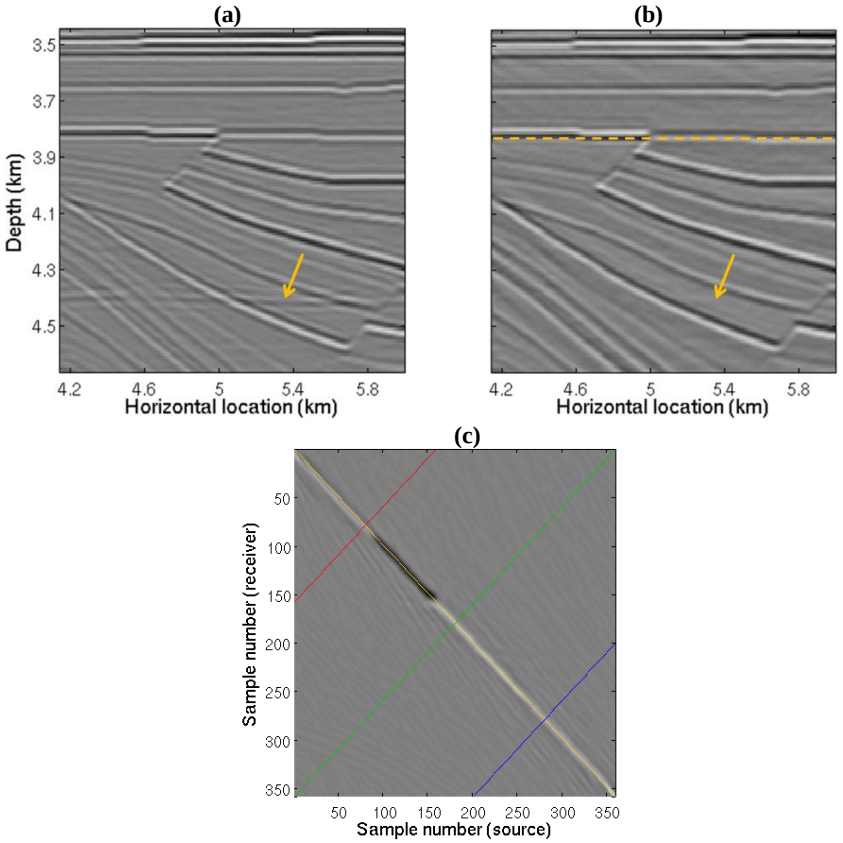

Figure 3: Panel (a) shows the subsurface image obtained using the cross-correlation imaging condition. The arrow indicates a strong cross-talk event (replication of the sea bottom). Panel (b) is the zero-offset section obtained after computing the reflectivity matrix. The yellow dashed line indicates the depth level where we have computed the reflectivity (in frequency-space) of panel (c). Panel (c) is obtained after extraction of the zero time-lag and is overlaid in yellow by the subset used to build the zero-offset section of panel (b). The red, green and blue lines indicate the subsets used to build the common-midpoint sections and angle gathers of Figure 4.

DOI http://dx.doi.org/10.1190/segam2015-5828037.1

shifted towards the left side of the display, corresponding to the dipping events.

Conclusions

For migration approaches employing the complete wavefield (including primaries and multiples), multiple scattering wave paths may lead to cross-talk artifacts, if they are not properly suppressed. In this study, based on the Sigsbee2B model, we show how this can be accounted for through a scheme that explicitly inverts for the reflectivity of the subsurface. This approach reduces cross-talk in the structural migrated images, and can also be extended to produce angle gathers in the image point location. Further, the reflectivity can be used to obtain data corresponding to virtual sources and receivers located in the subsurface, at a given image level. The presented approach may be applied target oriented, i.e. the reflectivity may only be computed in the area of most interest.

Acknowledgements

We thank the Norwegian Research Council for their financial support and also PGS Geophysical AS and the Department of Geosciences of UiO for permission to present this work. Finally, we also thank Chiung-Chuan Cheng and Shaoping Lu from Petroleum Geo-Services for their contribution to this study.

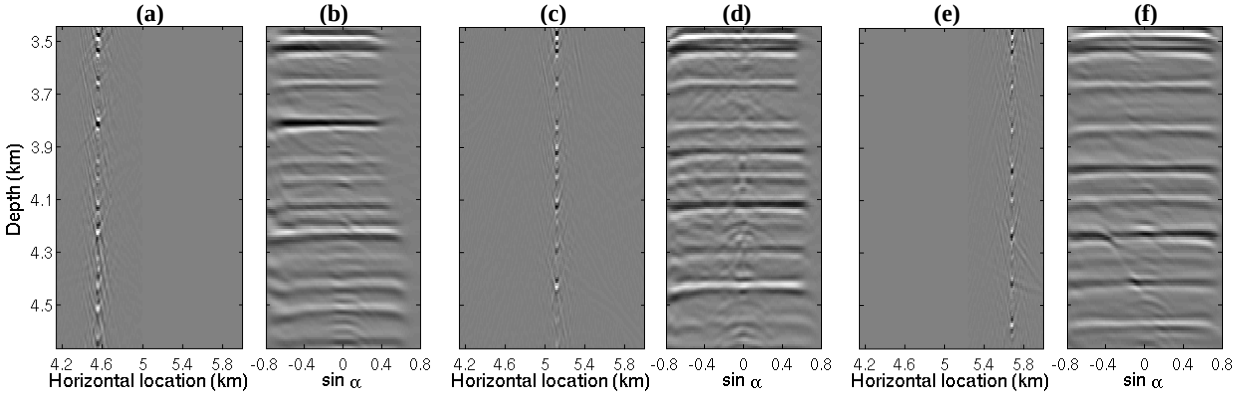

Figure 4: Panel (a) is a common-midpoint migrated section and panel (b) its corresponding angle gather. These panels have been determined at the lateral position colored in red in Figure 1b (i.e. extraction of the anti-diagonal colored in red in Figure 3c). Panels (c)-(d) and panels (e)-(f) are associated to the positions colored in green and blue in Figure 1b and Figure 3c, respectively.

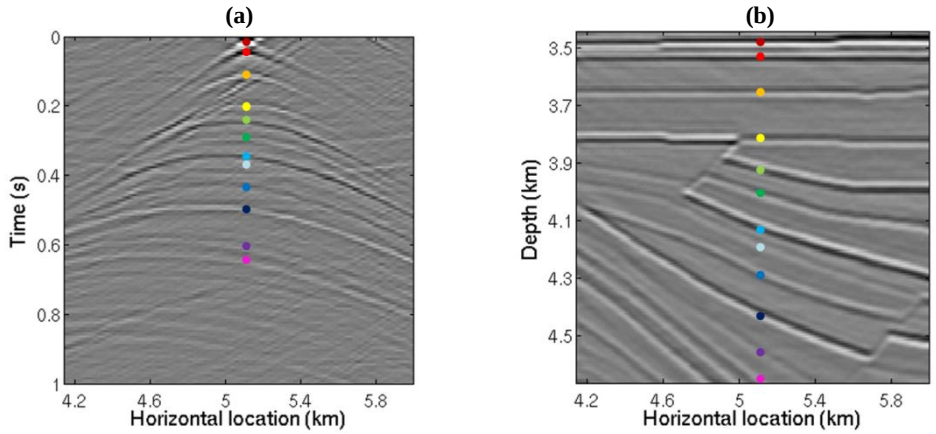

Figure 5: Panel (a) represents a shot record of the reflectivity wavefield as if it was generated by a source at the position indicated in Figure 1b. Panel (b) is the same as the zero-offset section of Figure 3b. The events appearing in the reflectivity shot record can be directly associated with the migrated layers, as indicated by colored dots.

DOI http://dx.doi.org/10.1190/segam2015-5828037.1

EDITED REFERENCES

Note: This reference list is a copyedited version of the reference list submitted by the author. Reference lists for the 2015 SEG Technical Program Expanded Abstracts have been copyedited so that references provided with the online metadata for each paper will achieve a high degree of linking to cited sources that appear on the Web.

REFERENCES

Amundsen, L., 2001, Elimination of the free-surface related multiples without need of the source wavelet: Geophysics, **66**, 327–341, http://dx.doi.org/10.1190/1.1444912.

Berkhout, A. J., 1985, Seismic migration: Imaging of acoustic energy by wave field extrapolation: Elsevier Science Publ. Co.

Berkhout, A. J., and D. J. Verschuur, 2003, Transformation of multiples into primaries: 73rd Annual International Meeting, SEG, Expanded Abstracts, 1925–1928.

Claerbout, J. F., 1971, Toward a unified theory of reflector mapping: Geophysics, **36**, 467–481, http://dx.doi.org/10.1190/1.1440185.

de Bruin, C. G. M., C. P. A. Wapenaar, and A. J. Berkhout, 1990, Angle-dependent reflectivity by means of prestack-migration: Geophysics, **55**, 1223–1234, http://dx.doi.org/10.1190/1.1442938.

Guitton, A., A. A. Valenciano, D. Bevc, and J. Claerbout, 2007, Smoothing imaging condition for shot-profile migration: Geophysics, **72**, no. 3, S149–S154, http://dx.doi.org/10.1190/1.2712113.

Lu, S., N. D. Whitmore, A. A. Valenciano, and N. Chemingui, 2011, Imaging of primaries and multiples with 3D SEAM synthetic: 81st Annual International Meeting, SEG, Expanded Abstracts, 3217–3221, doi:10.1190/1.3627864.

Muijs, R., J. O. A. Robertsson, and K. Holliger, 2007, Prestack depth migration of primary and surface-related multiple reflections: Part I — Imaging: Geophysics, **72**, no. 2, S59–S69, http://dx.doi.org/10.1190/1.2422796.

Ordoñez, A., W. Söllner, T. Klüver, and L. J. Gelius, 2014a, Migration of primaries and multiples using an imaging condition for amplitude-normalized separated wavefields: Geophysics, **79**, no. 5, S217–S230, http://dx.doi.org/10.1190/geo2013-0346.1.

Ordoñez, A., W. Söllner, T. Klüver, and L. J. Gelius, 2014b, Recovering the reflectivity matrix and angle-dependent plane-wave reflection coefficients from imaging of multiples: 84th Annual International Meeting, SEG, Expanded Abstracts, 4066–4070.

Paffenholz, J., B. McLain, J. Zaske, and P. Keliher, 2002, Subsalt multiple attenuation and imaging: Observations from the Sigsbee2B synthetic dataset: 72nd Annual International Meeting, SEG, Expanded Abstracts, 2122–2125, doi:10.1190/segam2014-1049.1.

Poole, T. L., A. Curtis, J. O. A. Robertsson, and D. J. van Manen, 2010, Deconvolution imaging conditions and cross-talk suppression: Geophysics, **75**, no. 6, W1–W12, http://dx.doi.org/10.1190/1.3493638.

Posthumus, B., 1993, Deghosting of twin streamer configuration: Geophysical Prospecting, **41**, no. 3, 267–286, http://dx.doi.org/10.1111/j.1365-2478.1993.tb00570.x.

Tikhonov, A. N., A. V. Goncharsky, V. V. Stepanov, and A. G. Yagola, 1995, Numerical methods for the solution of ill-posed problems: Kluwer Academic Publishers, http://dx.doi.org/10.1007/978-94-015-8480-7.

Verschuur, D. J., and A. J. Berkhout, 2009, Target-oriented, least-squares imaging of blended data: 79th Annual International Meeting, SEG, Expanded Abstracts, 2889–2893.

Wapenaar, K., E. Slob, and R. Snieder, 2008, Seismic and electromagnetic controlled-source interferometry in dissipative media: Geophysical Prospecting, **56**, no. 3, 419–434, http://dx.doi.org/10.1111/j.1365-2478.2007.00686.x.

Wapenaar, K., J. van der Neut, and J. Thorbecke, 2012, On the relation between seismic interferometry and the simultaneous-source method: Geophysical Prospecting, **60**, no. 4, 802–823, http://dx.doi.org/10.1111/j.1365-2478.2012.01056.x.

Whitmore, N. D., A. A. Valenciano, W. Söllner, and S. Lu, 2010, Imaging of primaries and multiples using a dual-sensor towed streamer: 80th Annual International Meeting, SEG, Expanded Abstracts, 3187–3192.